Available online at www.sciencedirect.com
SCIENCE DIRECT
Journal of Chromatography A, 1094 (2005) 148–157
JOURNAL OF CHROMATOGRAPHY A
www.elsevier.com/locate/chroma

Expanded electrical model of a contactless conductivity detector: Development and verification

Stephen E. Johnston, Keith E. Fadgen [1], Luke T. Tolley [2], James W. Jorgenson *

Department of Chemistry, University of North Carolina at Chapel Hill, Venable Hall, CB#3290, Chapel Hill, NC 27599-3290, USA

Received 10 May 2005; received in revised form 8 July 2005; accepted 25 July 2005
Available online 18 August 2005

Abstract

A theoretical model of the contactless conductivity detector (CCD) has been developed consisting of a network of resistors and capacitors. The output of the model is compared to experimental results and to the output of a simpler model. Experimentally, a lock-in amplifier is added to the detection scheme of the contactless conductivity detector to provide a more sensitive method of signal isolation. The detector is assembled on a printed circuit board with the electrodes in a co-axial configuration. The electrodes are chosen to allow for use with fused silica capillaries in capillary electrophoresis. The use of a lock-in amplifier in place of a previous rectification/filtering circuit allows for an approximate 10-fold improvement in S/N. The detector shows a linear response to changes in excitation voltage and to changes in analyte concentration. Mass limits of detection of 60, 63, and 50 fg are determined for the inorganic cations potassium, sodium, and lithium, respectively (for a signal three times the level of the rms noise).

Keywords: Capillary electrophoresis; Contactless conductivity detection; Inorganic cations

1. Introduction

Although traditional UV absorbance detection techniques, both direct and indirect, are the most common detection techniques utilized in capillary electrophoresis, they are limited by the path length sensitivities inherent in absorbance detection. To combat this problem, several groups have, over the past several years, developed a capacitively-coupled, contactless conductivity detector (CCD) for use with capillary electrophoresis. Although the detailed design of the CCD varies from group to group, the basic theory remains the same. Two electrodes are placed near each other on the outside of a capillary with an alternating current signal applied to one of the electrodes. The signal is capacitively coupled through the silica capillary wall and into the ionically conductive liquid core of the capillary. The signal is then conducted through the liquid core until it reaches the other electrode, where it is capacitively coupled back out through the silica wall. The CCD is an improvement over previous on-column conductivity detectors in that the conductivity measurement is made without direct contact with the liquid and without modification of the capillary.

The basic principle of the contactless conductivity detector was first described in 1980 by Gas et al. [1], for use as a high-frequency detector for isotachophoresis. This original design consisted of four electrodes placed radially around the separation column. In 1998, Zemann et al. [2] developed a new version of the CCD consisting of two electrodes placed axially on the column. The electrodes, 30 mm in length and separated by 2 mm, could be either made from syringe cannulas, or painted on the capillary using a conductive silver varnish. A 40 kHz, 8 Vp-p sinusoidal excitation signal was applied to one of the electrodes, with

* Corresponding author. Tel.: +1 919 966 5071; fax: +1 919 962 1381/2388.
E-mail address: jj@unc.edu (J.W. Jorgenson).
[1] Present address: Waters Corporation, 34 Maple St., Mail Stop CT, Milford, MA 01757, USA.
[2] Present address: Southern Illinois University, Department of Chemistry, 1245 Lincoln Dr., Mailstop 4409, Carbondale, Il 62901, USA.

0021-9673/$ – see front matter © 2005 Elsevier B.V. All rights reserved.
doi:10.1016/j.chroma.2005.07.098

the detected signal amplified, rectified, and fed into a data acquisition and processing system. Independently, Fracassi da Silva and do Lago [3] published a comparable detector using 2 mm silver electrodes painted on the capillary with a 1 mm gap. They also added a ground plate between the electrodes to reduce direct capacitive coupling between the electrodes.

Since these initial papers, the effects of various experimental parameters have been investigated by several groups. These include cell geometry [4–6], high voltage excitation [7–9], excitation frequency [10,11], and electrode fabrication [12]. Miniaturization of the detector has also been advanced [13–16]. Applications have ranged from amino acid detection [17] and detection in UV-absorbing solvents [18–21], to inorganic ion analysis [22–29].

The circuit design for the initial reported contactless conductivity detector [2] was very simple. The output of the detection electrode was connected to ground through a resistor. The voltage drop across the resistor was then amplified, rectified, and measured. The first change made was the use of a current-to-voltage converter (transimpedance amplifier) in place of the grounded resistor [3]. A second change to the detection scheme was proposed by Guijt et al. [14] in 2001. Previously, rectification of the detected signal had been carried out using diodes. Guijt et al., instead, used a lock-in amplifier to achieve phase-sensitive detection, improving the noise discrimination of the system. In the original rectifier circuit, no frequency selective component is present until the low pass filter. Noise at all frequencies within the wide bandwidth of the amplifier is passed on to the rectification circuit and thus folds in with the desired signal. The lock-in amplifier allows for isolation of the frequency of interest within a narrow bandwidth before detection, while ignoring all other frequencies.

The work presented herein further expands upon the benefits of using a lock-in amplifier in the detection scheme. Detector response as a function of excitation potential and analyte concentration was investigated along with the noise characteristics of the detector. An equivalent electrical circuit for the conductivity cell is also proposed to allow for a better understanding of the factors affecting the cell output.

2. Experimental

2.1. Materials

Potassium chloride and sodium chloride were obtained from Mallinckrodt (Paris, KY). Lithium chloride was obtained from Fisher Scientific (Fair Lawn, NJ). L-Histidine and 2-[*N*-morpholine]ethanesulfonic acid hydrate (MES) were obtained from Sigma (St. Louis, MO). All compounds were used as received. Deionized water was obtained from a Barnstead Nanopure System (Boston, MA). The CE run buffer used was 20 mM MES/20 mM Histidine, pH 5.9 prepared in deionized water. Buffer solutions were filtered using a 0.2 μm nylon membrane filter from Alltech Associates (Deerfield, IL), then vacuum degassed.

2.2. Capillary electrophoresis system

CE was performed in an untreated fused silica capillary (Polymicro Technologies, Phoenix, AZ) with an inner diameter of 50 μm, an outer diameter of 360 μm, and a length of 68 cm. Sample was injected electrokinetically at 2 kV for 4.5 s. A 30 kV dc, reversible polarity power supply (Spellman High Voltage Electronics Corp., Plainview, NY) was used in the positive mode.

2.3. Contactless conductivity detector

There were two designs of the contactless conductivity detector used in this work. The design used for the voltage and concentration studies (design 1) is similar to previously published designs [3], but with some modifications. The cylinders used for electrodes are 23 gauge, 304 stainless steel hypo tubing (Small Parts, Miami Lakes, FL) drilled out to an inner diameter of 390 μm and cut to lengths of 5 mm. A single conductivity cell is formed when two electrodes are soldered to a printed circuit board (ExpressPCB, Redwood City, CA) with a 1.1 mm gap between them. The op-amp used in the current-to-voltage converter is an OPA602A (Texas Instruments, Dallas, TX) which was chosen for its low current noise characteristics. The 1 MΩ feedback resistor for the current-to-voltage converter is a thin film resistor chosen for its precision and temperature stability.

An SR810 digital signal processor (DSP) lock-in amplifier (Stanford Research Systems, Sunnyvale, CA) is used for signal isolation and amplification. The external reference signal is provided to the lock-in amplifier by a DS335 function generator (Stanford Research Systems, Sunnyvale, CA). The function generator is set to output 20 Vp-p at 100 kHz and is used both as the reference for the lock-in amplifier and as the excitation source for the contactless conductivity detector. These settings are used for all separations unless otherwise noted. A 100 kHz excitation frequency was chosen due to the 102 kHz frequency limit of this lock-in amplifier. The output of the lock-in amplifier is digitized by a PCI-MIO-16XE-50 data acquisition card (National Instruments, Austin, TX) in a personal computer. Data points are collected and analyzed on the computer by custom software written in LabVIEW (National Instruments, Austin, TX) and Igor Pro (WaveMetrics, Lake Oswego, OR). The results from each CE run are median filtered baseline subtracted [30] prior to any calculations being performed.

The contactless conductivity detector used to compare experimental results to theoretical calculations (design 2) was designed to reduce the leakage capacitance between the electrodes. The detector consists of a stainless steel cylinder, through which a hole is bored just large enough that 1/16″

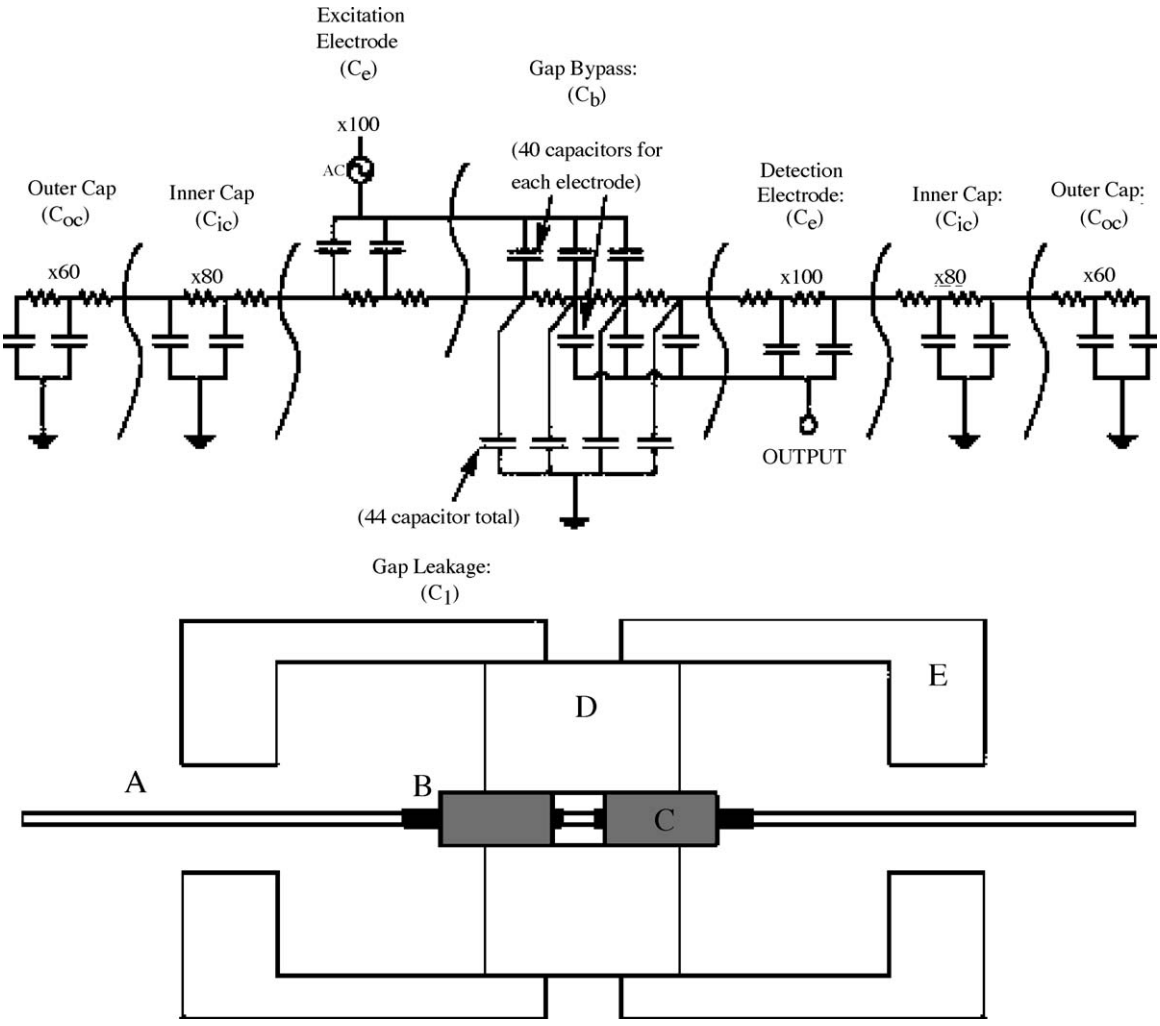

Fig. 1. Description of electrical circuit used to model contactless conductivity cell. The cell is broken into 25 μm wide segments (1044 total) with each segment containing a resistance and at least one capacitance. Below is the corresponding diagram of the cell used to compare experimental data to the model. (A) capillary; (B) electrodes; (C) Teflon tubing; (D) cylindrical stainless steel ground; and (E) endcap stainless steel ground. The numbers above each section of the circuit (i.e. × 60) refer to the number of times that section is repeated in the complete model. For the outer cap, the two resistor-two capacitor pairing is repeated 60 times for a total of 120 resistors and capacitors in that section.

outer diameter Teflon tubing (Alltech, Deerfield, IL) can be thread into it. The same 5 mm long stainless steel electrodes used in the other design are fit inside the Teflon tubing and the capillary thread through the electrodes. Small diameter coaxial cable (Belden, Richmond, IN) is soldered onto the electrodes to bring in and carry away signal. Stainless steel endcaps are then fitted around the entire system to prevent leakage between the exposed portions of the electrodes. A diagram of the cell is shown in Fig. 1. The current-to-voltage converter was removed from the circuit to allow for measurements to be made without interference from the bandwidth limitations of the op-amp. The signal from the detection electrode was isolated and amplified using an SR844 RF lock-in amplifier (Stanford Research Systems, Sunnyvale, CA). Signal digitization, collection, and manipulation were performed as in design 1.

3. Theoretical

3.1. Equivalent simple electrical circuit of the contactless conductivity detector

A simple electrical model of the CCD can be constructed using the capillary wall capacitance, bulk solution resistance, and bypass capacitance between the electrodes (Fig. 2) [3]. However, this simple model fails to accurately predict the output of the cell. A more extensive spatial RC network was thus constructed to try and predict the output of the conductivity cell with a greater degree of accuracy (Fig. 1). This network is similar in structure to that previously proposed by Gas et al. [4].

The simple model was solved by reducing the circuit to a single series resistor/capacitor combination. The reduction

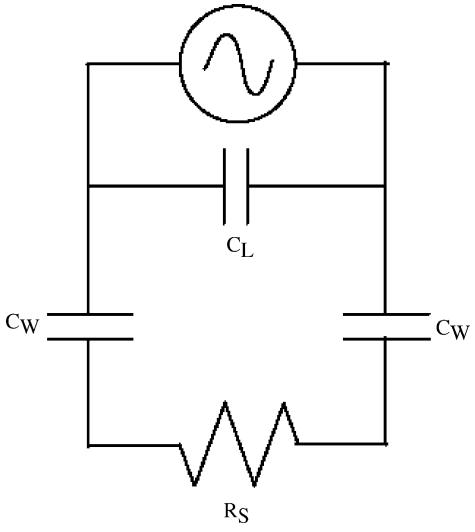

Fig. 2. Simple electrical circuit model of contactless conductivity detector where C_L is the leakage capacitance, C_W, the wall capacitance; and R_s, the solution resistance. The circuit is similar to that originally described [3] except the wall capacitance is split into two separate capacitances.

was performed using

$$R_p = \frac{R_s^2 + X_s^2}{R_s} \quad (1)$$

$$X_p = \frac{R_s^2 + X_s^2}{X_s} \quad (2)$$

$$R_s = \frac{R_p}{1 + (R_p/X_p)^2} \quad (3)$$

$$X_s = \frac{R_s R_p}{X_p} \quad (4)$$

where R_s is the series resistance; X_s, the series reactance; R_p, the parallel resistance; and X_p the parallel reactance [31]. These equations are used to convert a series *RX* (resistance/reactance) circuit to its parallel equivalent and vice versa. A stepwise example using the equations can be found in the reference [31]. For the conductivity cell, the wall capacitance and solution resistance, originally in series, are converted to their parallel equivalent. This puts them both parallel to the bypass capacitance. The equivalent parallel capacitance is then added to the bypass capacitance giving a single capacitance. This capacitance and the equivalent series capacitance are then converted to their series equivalent from which an impedance can be calculated.

The values for each resistance and capacitance were determined from experimental measurements. The solution resistance in the gap was calculated to be 12.43 MΩ (from the bulk resistance for a 68 cm long capillary). Considering the electrode and solution to be two concentric cylinders, the capillary wall capacitance was calculated to be 515 fF using

$$C = \frac{2\pi\varepsilon_c\varepsilon_o L}{\ln(r_e/r_{id})} \quad (5)$$

with ε_c the relative permittivity of the silica capillary wall; ε_o, the permittivity of free space; L, the electrode length; r_e, the inner radius of the electrode; and r_{id} the radius of the capillary inner diameter. The slight air gap between the outer capillary wall and the electrode is negligible and was ignored. From Eq. (6) (the capacitance between two parallel plates), the bypass current between the electrodes was calculated to be 1.1 fF.

$$C = \frac{\varepsilon_o A}{d} \quad (6)$$

with A the area of the ring face of the electrodes and d, the distance between the electrodes (gap distance). This value was confirmed experimentally by measurements of current through the cell in the absence of a capillary, and with acetone and deionized water-filled capillaries.

For a 7 V_{rms}, 100 kHz input, a circuit impedance of 13.82 MΩ was calculated using Eqs. (1)–(4) and the values calculated above, giving an output current of 0.51 μA. The calculated output current was then dropped across a 50 Ω resistor to model the input to the lock-in amplifier. A signal with a magnitude of 25.32 μV at a phase of 26.95° relative to the input signal was thus expected at the output of the simple circuit. Experimentally, a signal of magnitude 7.89 μV at a phase of 22.81° was measured using detector design 2. The measured signal magnitude was approximately three times smaller than predicted by the simple circuit (when modeled using experimental values).

3.2. Equivalent complex electrical circuit of the contactless conductivity detector

For the complex model, the entire cell was spatially divided into individual 25 μm long segments. Models were developed with spatial resolutions greater and less than 25 μm; however, it was determined that resolutions finer than 25 μm provided no further significant changes. Each segment was assigned a resistance and capacitance. The resistance (R_s) is determined by dividing up the bulk solution resistance for the entire capillary equally into the corresponding resistance for a 25 μm segment. The capacitance depends on what position in the cell the segment occupies. Five capacitances were considered: from the solution to the inner (larger) endcap radius (C_{ic}), solution to the outer (smaller) endcap radius (C_{oc}), electrode to solution (C_e), leakage from the solution in the gap to ground (C_l), and bypass between electrodes across the gap (C_b) (Fig. 1). The electrode to solution capacitance was determined using Eq. (5). With the exception of the bypass between the electrodes, the other capacitances were determined using:

$$C = \frac{2\pi\varepsilon_c\varepsilon_a\varepsilon_o L}{\varepsilon_a \ln(r_{od}/r_{id}) + \varepsilon_c \ln(r_g/r_{od})} \quad (7)$$

with ε_a the relative permittivity of air; r_{od}, the radius of the capillary outer diameter; and r_g, the inner radius of the ground cylinder. The bypass capacitances between the elec-

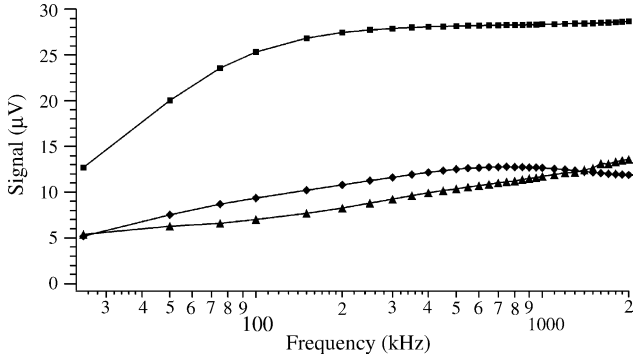

Fig. 3. Comparison of theoretical models to experimental output over the frequency range 25–2000 kHz: (■) simple model; (♦) 25 μm segment model; (▲) experimental results.

trodes were calculated using the tangential distance between the gap segment and the tip of the electrode. These distances (through silica and air) were used with Eq. (7) to determine an approximate capacitance. This gave the capacitances from one electrode to the other side of the gap a trend like that of a $1/\ln(x)$ curve. A capacitance of approximately 1.3 fF from an electrode to the furthest part of the gap is calculated. This value of the bypass capacitance approximately matches that previously calculated and experimentally determined.

Using Kirchoff's Laws, current and voltage equations were set up for each element and node. These equations were compiled in a square matrix and solved simultaneously using MATLAB (Mathworks, Natick, MA). The currents across the capacitances associated with the detection electrode were summed and dropped across a theoretical 50 Ω resistor to give an output voltage of 9.35 μV at a phase of 27.52°. This voltage was compared with the experimental output of the cell (detector design 2) detected using the 50 Ω input of the RF lock-in amplifier. The matrix method was chosen over the simple model solution method due to the presence of three nodes in the circuit (input, output through the left shielding cap, output through the detection electrode and right shielding cap), which prevented the reduction of the circuit to a single series resistor/capacitor combination.

A graphical comparison of the outputs of the simple model, our complex model, and the experimental cell is shown in Fig. 3 for a 1.1 mm gap and 50/360 capillary filled with 20 mM MES/his buffer. In the range 25–2000 kHz, the simple model predicts an output signal much larger than that seen experimentally. The complex model gives a much closer fit to the experimental data. The phase of the output signal relative to the AC excitation voltage was also compared, with the complex model again giving a much closer fit to experimental data. It should be noted that none of the resistance or capacitance values used in predicting the output of the simple or complex model were adjusted to obtain a better fit to the experimental data. The values used in each model were calculated using experimental measurements, with the components of the model (i.e. more segments, leakage to shielding cap ground) then adjusted to provide a better fit.

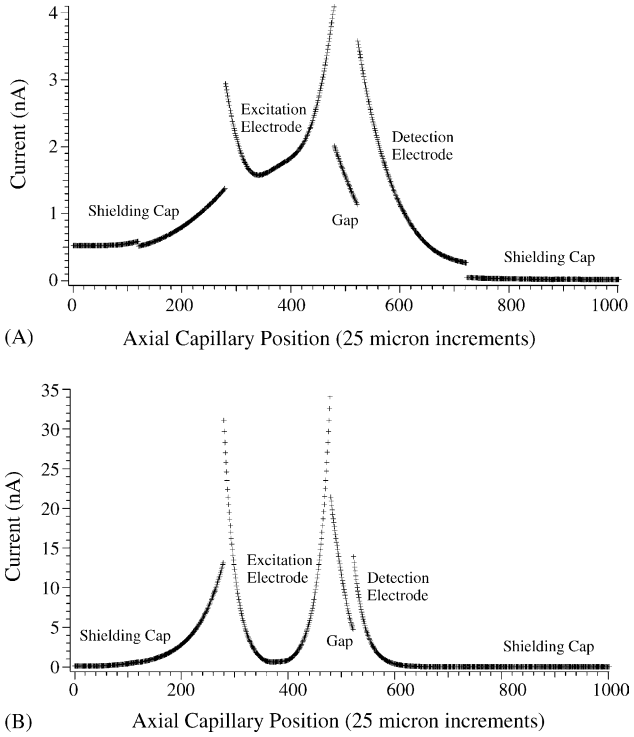

Fig. 4. Theoretical current flow through the cell as a function of position. Current flows at frequencies of 100 kHz (A) and 1 MHz (B) are shown. The current flow at 1 MHz is almost an order of magnitude larger than that at 100 kHz. Current flow is for a 50/360 capillary with a 1.1 mm gap and 5 mm electrodes. Sections of current flow are labeled to correspond with the section of the cell the current is flowing through.

For the simple model, adjustment of the actual values was attempted, with no reasonable values giving a better fit to the experimental data than the actual values in the complex model do.

Using the complex model, the current flow through each segment of the cell can also be modeled. Fig. 4 shows the current flow as a function of position in the cell for excitation at 100 kHz and 1 MHz. It can be seen that theoretically, more current flows through the cell at the higher frequency. At 1 MHz, current flows from and into the electrodes mainly at the tips of the electrodes. At 100 kHz, current flows more evenly across the entire electrode. This suggests that at higher frequencies, a shorter electrode can be used without losing any sensitivity in detection, while at lower frequencies, longer electrodes are needed in order to increase sensitivity. This is a direct result of decreasing capacitive reactance (impedance) at higher frequencies. The current flow is also seen to be asymmetrical around the excitation electrode due to the differing pathways to ground on each side of the electrode.

The effects of the capillary inner diameter and the size of the gap were also modeled. Capillary inner diameters of 25, 50 and 100 μm were modeled and then experimentally tested with the results shown in Fig. 5. The model and experimental data follow closely across the frequency range for all three diameters with the larger diameter giving a larger signal as would be expected due to the increase in area occupied by the

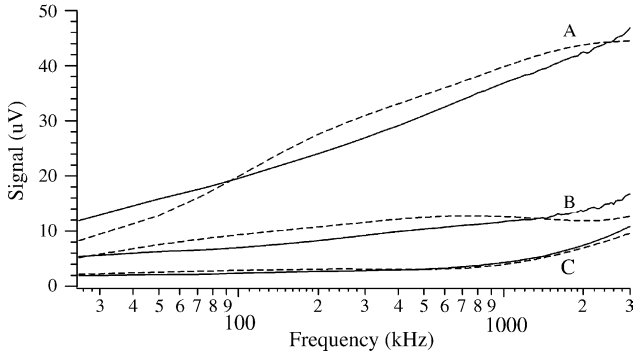

Fig. 5. Effect of capillary inner diameter on response of cell. Traces are for (A) 100 μm; (B) 50 μm and; (C) 25 μm inner diameters. Solid lines are the experimental data while dashed lines are the modeled data. The capillary outer diameter is 360 μm with a gap size of 1.1 mm and 5 mm long electrodes in all cases.

conductive solution. The model and experimental results for the size of the gap also match each other, with the smaller gap giving a larger signal, due to a smaller resistance between the electrodes in the capillary core and also a larger capacitive bypass current.

4. Results and discussion

4.1. Advantages of lock-in based system over previous designs

A circuit consisting of separate amplification, rectification, and filtering steps was assembled. The voltage drop across a 47 kΩ resistor was sent to an instrumentation amplifier (model INA103, Texas Instruments, Dallas, TX) with an internal gain of 100, followed by a diode/capacitor rectification circuit. The final step was a low-pass Sallen-Key filter set to 22 Hz (equivalent noise bandwidth of 2.75 Hz) followed by a second order digital RC filter with a 0.2 s time constant (0.80 Hz bandwidth). Using this design, a separation of 50 ppm potassium, sodium, and lithium ions was performed with an observed S/N of 73, 76, and 97, respectively (Fig. 6A). When the rectification and filter circuits were replaced with the Stanford Research model 810 lock-in amplifier set at a 0.78 Hz equivalent noise bandwidth (100 ms time constant, 24 dB/oct filter slope), the same separation was performed with an observed S/N of 842, 725, and 1130, respectively (Fig. 6B). This is an approximate order of magnitude improvement in S/N over the rectification/filter circuit.

4.2. Cell response as a function of excitation potential

A 10.0 ppm mixture of potassium, sodium, and lithium ions was separated and detected using the contactless conductivity detector. Sinusoidal excitation signals were generated at 1 and 20 Vp-p with an excitation frequency of 100 kHz in each case. The increases in peak area, peak height, and

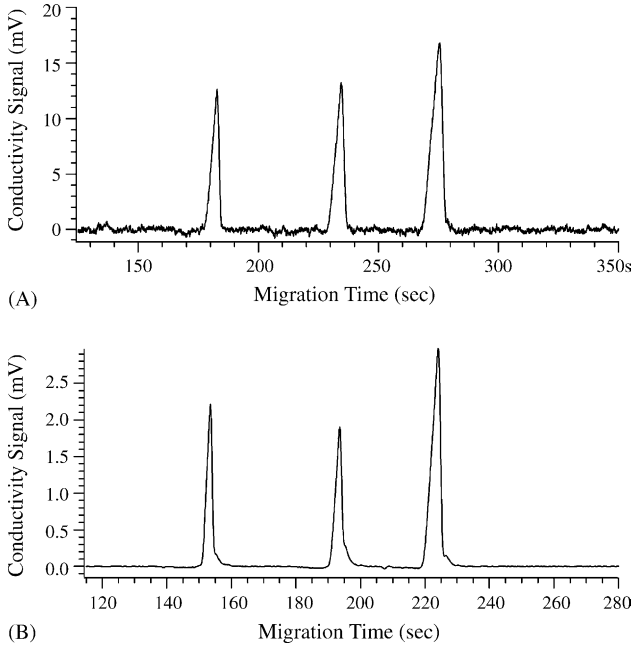

Fig. 6. Effect of the lock-in amplifier on the noise of the system. An amplifier/rectifier/filter circuit was used to detect the separation of a 50 ppm solution of K^+, Na^+, and Li^+ (A). The same separation was detected using a lock-in amplifer (B). A digital filter was applied to the non-lock-in amplifier data in order to compare equivalent bandwidths. The migration times differ due to different lengths of capillary used. Separation conditions: 20 mM MES/his, pH 6.0 buffer, 20 kV.

baseline noise are summarized in Table 1. It is seen that signal response increases as a function of excitation potential. For potassium, the peak area shows an increase of 20.7× from 1 Vp-p to 20 Vp-p. The theoretical improvement in signal response is 20.0× for this voltage change. The observed increase is a good match to the theoretical increase. The same match between the observed and theoretical increase was also seen for the other two analytes, sodium and lithium.

As the excitation voltage increases, so does the noise. Under shot noise limited conditions (shot noise of the background conductivity current), the baseline noise should scale as the square root of the increase in background current, which is proportional to the excitation voltage. The observed noise increase is greater than this theoretical expectation. The likely explanation for this is amplitude instability in the excitation source (function generator). A noise value of

Table 1
Comparison of measured and theoretical increases for potassium ion due to an increase in excitation voltage[a]

	Signal increase factor	
	Experimental	Theoretical
Peak area	20.72	20
Peak height	20.28	20
Baseline noise	9.93	4.47

[a] Similar increases were seen for sodium and lithium ions.

Table 2
Noise instability of function generator relative to excitation voltage

	7.07 V_{rms} excitation	0.354 V_{rms} excitation
Voltage detected by lock-in	380 mV	19 mV
Current at detection electrode	380 nA	19 nA
Impedance of cell	18.6 MΩ	18.6 MΩ
Amplitude instability of function generator (0.001%)	70.7 μV	3.54 μV
Current noise resulting from function generator instability	3.8 pA	0.19 pA
Voltage noise resulting from function generator instability	3800 nV	190 nV
Shot noise in detection electrode current	800 nV	180 nV
Johnson noise of feedback resistor	164 nV	164 nV
Lock-in amplifier noise	7.6 nV	7.6 nV
Op-amp voltage noise	29 nV	29 nV
Op-amp current noise	0.78 nV	0.78 nV
Expected total noise from all contributions	3800 nV	310 nV
Overall noise detected by lock-in	2800 nV	300 nV

approximately 0.001% of the signal magnitude was experimentally measured for the excitation source using a lock-in amplifier set to the same time constant as used in conductivity detection. This linear increase in noise magnitude with a linear increase in signal magnitude could account for the larger than expected increase at higher voltages, as the noise resulting from the 0.001% amplitude instability in the source becomes significant relative to other noise sources. As shown in Table 2, the noise increase expected due to a 0.001% instability in the voltage source is comparable to the noise increase observed experimentally when using higher voltages.

The background voltage detected by the lock-in using a 7.07 V_{rms} input voltage is 380 mV. This corresponds to a current at the detection electrode of 380 nA (10^6 gain on the current-to-voltage converter), giving a cell impedance of 18.6 MΩ. An 0.001% instability in the 7.07 V input voltage corresponds to a 70.7 μV instability. Using the cell impedance just calculated earlier, a current noise of 3.8 pA is seen at the detection electrode resulting from the instability of the function generator, with the lock-in amplifier detecting a signal of 3800 nV (voltage noise resulting from function generator instability) following the 10^6 gain in transimpedance amplifier. Johnson noise in the op-amp feedback resistor is 164 nV. The lock-in amplifier adds 7.6 nV of noise [32], while the op-amp contributes 29 nV of voltage noise and 0.78 nV of current noise [33]. The shot noise in the current at the detection electrode is 800 nV.

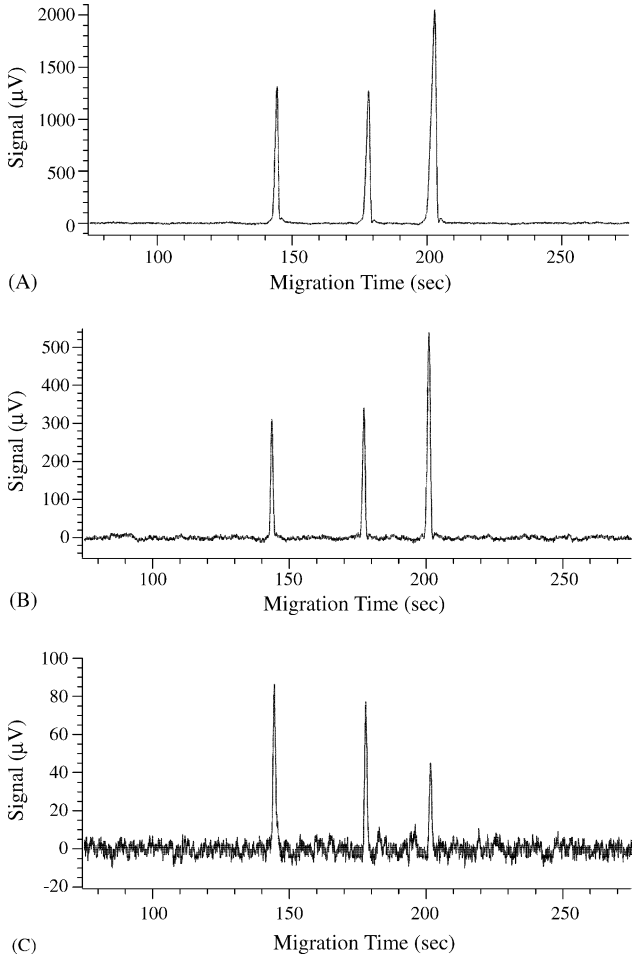

Fig. 7. Electropherograms obtained for (A) 7.0; (B) 1.0; and (C) 0.1 ppm solutions of potassium, sodium, and lithium ions. Separations were performed in 20 mM MES/his buffer, pH 6.0 with a 20 kV separation voltage.

Table 3
Results of linear regression analyses on the log–log peak area data for inorganic cations[a]

	Potassium	Sodium	Lithium
Including all concentrations			
Slope	0.66	0.75	1.07
Intercept	−3.41	−3.39	−3.22
Without lower concentrations			
Slope	0.86	0.86	1.04
Intercept	−3.48	−3.42	−3.22

[a] The two lowest concentrations tested (0.05 and 0.1 ppm) are non-linear compared to the other concentrations. The regression analysis was performed both with and without these concentrations. A slope of 1.00 indicates a linear relationship between the variables. The intercept is of the form "log *a*" where "*a*" is a response factor for the system for the particular analyte.

Table 4
Summary of contactless conductometric inorganic cation detection in the literature

Reference	Capillary I.D. (μm)	Buffer	Voltage (V_{p-p})	Frequency (kHz)	Signal filtering[a]	Concentration LOD (ppb)			Mass LOD (fg)[b]		
						K^+	Na^+	Li^+	K^+	Na^+	Li^+
[2]	50	20 mM MES/his	8	40	Not specified		200			600	
[3]	75	10 mM MES/his	20	600	Low pass (159 Hz)	43	37	10	2100	1800	510
[5]	50	20 mM MES/his, 1 mM 18-crown-6	11	100	Smoothing (moving average)	35	36	21	300	310	180
[5]	75	20 mM MES/his, 1 mM 18-crown-6	11	100	Smoothing (moving average)	15	13	7	660	570	310
[5]	75	10 mM MES/his, 1 mM 18-crown-6	11	100	Smoothing (moving average)	9	8	4	390	350	170
[26]	75	20 mM boric acid, 10 mM LiOH	10	200	Low pass (159 Hz)	3.9			68		
[12]	75	20 mM MES/his	20	200	Not specified	20			770		
[11]	75	10 mM MES/his	2	600	Low pass (159 Hz)	43	37	10	2100	1800	510
[7]	75	10 mM MES/his	250	190	Low pass	5	5	2	120	96	35
[22]	75	50 mM MES/his, 1 mM 18-crown-6	11	100	Not specified			70			780
[27]	50	20 mM MES/his, 1.5 mM 18-crown-6	20	290	Low pass (159 Hz)	13	11	7	200	170	110
[10]	50	20 mM MES/his	n/a	100	Low pass (159 kHz), lock-in[c]	12		2	52		9
[24]	50	8 mM His, 2.8 mM HIBA, 0.32 mM 18-crown-6	10	290	Low pass (159 Hz)	15	7.5	7.5	160	78	78
[9]	75	10 mM MES/his, 2.5 mM 18-crown-6	300	100	Low pass (100 Hz)	1.5	0.7	0.9	38	15	16
[28]	75 (PEEK)	10 mM MES/his, 1 mM 18-crown-6	450	100	Low pass	4.7	1.7	1.1	87	31	21
[23]	75	20 mM MES/his, 2.5 mM 18-crown-6	20	1100	Low pass (159 Hz)	17	9.4		850	470	
[29]	50	20 mM MES/his	25	291	Low pass (16 Hz)	240	120	220	1200	590	1100
Present work	50	20 mM MES/his	20	100	Lock-in (0.78 Hz)	27	25	16	60	63	50

[a] Due to lack of information, accurate bandwidths could not be determined for all references.
[b] Limits of detection calculated from injection methods described in reference and ionic mobilities.
[c] Bandwidth is that reported for low pass filter, lock-in bandwidth not specified.

The square root of the sum of the squares of all noise contributions is thus 3800 nV. This is slightly more noise than is experimentally seen (2800 nV). The calculation was repeated at a 0.354 V_{rms} input voltage for comparison, yielding an expected noise of 310 nV (experimental noise was 300 nV). At the lower input voltage, Johnson noise in the op-amp feedback resistor, shot noise, and noise resulting from the function generator instability contribute equally to the overall noise. However, as the input voltage increases, the noise resulting from the function generator instability begins to dominate with the other sources of noise becoming negligible.

4.3. Cell response as a function of concentration

Mixtures of potassium, sodium, and lithium ions at various concentrations were separated and detected using the contactless conductivity detector. Concentrations of 0.05, 0.10, 0.20, 0.40, 1.00, 4.00, and 7.00 ppm were investigated for each analyte. An excitation voltage of 20 Vp-p was used for all concentrations. Sample electropherograms obtained for 7.0, 1.0, and 0.10 ppm are shown in Fig. 7. The average baseline noise seen was 2.8 μV_{rms}.

A linear regression analysis was performed on the potassium peak area data (in log–log form) from each individual run, giving a slope of 0.66. Linear regression analyses performed on the peak area data for the sodium and lithium peaks gave slopes of 0.75 and 1.07, respectively (Table 3). However, one problem with the data is the non-linear response at low concentrations of the potassium and sodium ions, which has been previously reported [12]. Due to this non-linear response, limits of detection are difficult to establish for these two ions. Removing the points at lower concentrations from the regression analysis of the cations, the slopes for potassium, sodium, and lithium become 0.86, 0.86, and 1.04, respectively. One possibility for the non-linear response of these two ions is their natural prevalence in the environment, making the accurate preparation of low concentration solutions difficult.

A summary of mass limits of detection found in the literature is shown in Table 4. Only those articles in which the mass limit could be determined are compared. Mass limits were chosen for comparison as they remove any bias caused by sample injection concentration or sample plug length. For the data presented herein, mass limits of 60, 63, and 50 fg were determined for potassium, sodium, and lithium ions, respectively, using a threshold of three times the rms noise level. These mass limits are slightly better than most of the other reported mass limits with the exception of those references where much higher excitation voltages were used. Compared to the other reported lock-in detection [10], the potassium mass limit is comparable while the lithium limit is slightly worse. This is probably due to the bias against lithium injection when using electrokinetic injection, as in our work, versus pressure injection, as in the work of Guijt and co-workers [10]. If a pressure injection technique had been used, the electrophoretic bias against lithium injection would have been eliminated and all ions would have been injected in equal amounts. However, an electrokinetic injection was found to produce more reproducible results.

Acknowledgments

This work was funded by a grant from the Waters Corporation and Grant CHE-9727505 from the National Science Foundation.

References

[1] B. Gas, M. Demjanenko, J. Vacik, J. Chromatgr. 192 (1980) 253.
[2] A.J. Zemann, E. Schnell, D. Volgger, G.K. Bonn, Anal. Chem. 70 (1998) 563.
[3] J.A. Fracassi da Silva, C.L. do Lago, Anal. Chem. 70 (1998) 4339.
[4] B. Gas, J. Zuska, P. Coufal, T. van de Goor, Electrophoresis 23 (2002) 3520.
[5] K. Mayrhofer, A.J. Zemann, E. Schnell, G.K. Bonn, Anal. Chem. 71 (1999) 3828.
[6] P. Tuma, F. Opekar, K. Stulik, Electrophoresis 23 (2002) 3718.
[7] J. Tanyanyiwa, B. Galliker, M.A. Schwarz, P.C. Hauser, Analyst 127 (2002) 214.
[8] J. Tanyanyiwa, P.C. Hauser, Anal. Chem. 74 (2002) 6378.
[9] J. Tanyanyiwa, P.C. Hasuer, Electrophoresis 23 (2002) 3781.
[10] E. Baltussen, R.M. Guijt, G. van der Steen, F. Laugere, S. Baltussen, G.W.K. van Dedem, Electrophoresis 23 (2002) 2888.
[11] J.A. Fracassi da Silva, N. Guzman, C.L. do Lago, J. Chromatogr. A 942 (2002) 249.
[12] P. Tuma, F. Opekar, I. Jelinek, Electroanalysis 13 (2001) 989.
[13] A. Berthold, F. Laugere, H. Schellevis, C.R. de Boer, M. Laros, R.M. Guijt, P.M. Sarro, M.J. Vellekoop, Electrophoresis 23 (2002) 3511.
[14] R.M. Guijt, E. Baltussen, G. van der Steen, H. Frank, H. Billiet, T. Schalkhammer, F. Laugere, M. Vellekoop, A. Berthold, L. Sarro, G.W.K. van Dedem, Electrophoresis 22 (2001) 2537.
[15] J. Lichtenberg, N.F. de Rooij, E. Verpoorte, Electrophoresis 23 (2002) 3769.
[16] M. Pumera, J. Wang, F. Opekar, I. Jelinek, J. Feldman, H. Lowe, S. Hardt, Anal. Chem. 74 (2002) 1968.
[17] P. Coufal, J. Zuska, T. van de Goor, V. Smith, B. Gas, Electrophoresis 24 (2003) 671.
[18] J. Muzikar, T. van de Goor, B. Gas, E. Kenndler, J. Chromatgr. A 924 (2001) 147.
[19] J. Muzikar, T. van de Goor, B. Gas, E. Kenndler, Anal. Chem. 74 (2002) 428.
[20] J. Muzikar, T. van de Goor, E. Kenndler, Anal. Chem. 74 (2002) 433.
[21] J. Wang, M. Pumera, Anal. Chem. 75 (2003) 341.
[22] V. Unterholzner, M. Macka, P.R. Haddad, A. Zemann, Analyst 127 (2002) 715.
[23] F.R. Rocha, J.A. Fracassi da Silva, C.L. Lago, A. Fornaro, I.G.R. Gutz, Atmos. Environ. 37 (2003) 105.
[24] P. Kuban, P. Kuban, V. Kuban, Electrophoresis 23 (2002) 3725.
[25] M. Masar, R. Bodor, D. Kaniansky, J. Chromatogr. A 834 (1999) 179.
[26] T. Chvojka, I. Jelinik, F. Opekar, K. Stulik, Anal. Chem. Acta 433 (2001) 13.
[27] P. Kuban, B. Karlberg, P. Kuban, V. Kuban, J. Chromatgr. A 964 (2002) 227.

[28] J. Tanyanyiwa, S. Leuthardt, P.C. Hauser, J. Chromatgr. A 978 (2002) 205.
[29] P.S. Vuorinen, M. Jussila, H. Siren, S. Palonen, M.-L. Riekkola, J. Chromatgr. A 990 (2003) 45.
[30] A.W. Moore, J.W. Jorgenson, Anal. Chem. 65 (1993) 188.
[31] D.G. Reed (Ed.), ARRL Handbook For Radio Communications 2004, ARRL, Newington, CT, 2003, p. 6.34.
[32] Users Manual, Model SR810 DSP Lock-In Amplifier, Stanford Research Systems.
[33] Specification Sheet, OPA602, Texas Instruments.